PHYSICAL REVIEW B **90**, 121403(R) (2014)

Giant room-temperature spin caloritronics in spin-semiconducting graphene nanoribbons

Xiaobin Chen,[1] Yizhou Liu,[1] Bing-Lin Gu,[1,2,3] Wenhui Duan,[1,2,3,*] and Feng Liu[1,2,4,†]

[1]*Department of Physics and State Key Laboratory of Low-Dimensional Quantum Physics, Tsinghua University, Beijing 100084, China*

[2]*Collaborative Innovation Center of Quantum Matter, Beijing 100084, China*

[3]*Institute for Advanced Study, Tsinghua University, Beijing 100084, China*

[4]*Department of Materials Science and Engineering, University of Utah, Salt Lake City, Utah 84112, USA*

(Received 21 April 2014; revised manuscript received 9 September 2014; published 22 September 2014)

Spin caloritronics refers to generating spin current by thermal gradient. Here we report a theoretical study demonstrating giant spin caloritronic effects in a new class of materials, called spin semiconductors, which are characterized with a "spin gap," the energy gap between spin-up and -down channels. Generally, spin Seebeck coefficient (S_s) is shown to increase linearly with the spin gap. Specifically, unprecedented large $S_s \sim 3.4$ mV/K and spin figure of merit $Z_sT \sim 119$ were found in spin-semiconducting graphene nanoribbons (GNRs) with sawtooth (ST) zigzag edges, based on first-principles calculations. Such giant spin caloritronic effects are shown to originate from a large spin gap of ST GNRs, in addition to two other spin-independent features of large band gap and narrow bandwidth which are commonly known for good thermoelectric materials. Our studies suggest that spin-semiconducting nanostructures, such as ST GNRs, are promising candidates for room-temperature spin caloritronics with high efficiency.

DOI: 10.1103/PhysRevB.90.121403 PACS number(s): 72.80.Vp, 65.80.Ck, 72.20.Pa, 85.75.−d

With the continuing development of spintronics, there is a growing interest in materials that can inject and/or carry spin current as a new means to transfer information efficiently [1,2]. It has been demonstrated that thermal energy can be used to generate spin current [3–6]. The conversion efficiency of such so-called spin caloritronic effect can be characterized by spin figure of merit as $Z_sT = |G_s|S_s^2T/(\kappa_e + \kappa_{ph})$, where $G_s = G_\uparrow - G_\downarrow$ is spin conductance, $S_s = S_\uparrow - S_\downarrow$ is spin Seebeck coefficient, G_σ (S_σ) is the spin-dependent electric conductance (Seebeck coefficient) of spin-σ electrons, and κ_e (κ_{ph}) is electronic (lattice) thermal conductance [7–9]. Recently, a new class of materials of spin semiconductors have been proposed [10]. A special property of spin semiconductors is that both spin channels are semiconducting and relatively energy shifted, resulting in a finite spin gap, i.e., an energy gap between spin-up and -down channels around the Fermi level. In this Rapid Communication, using spin-semiconducting sawtooth (ST) graphene nanoribbons (GNRs) as model systems, we demonstrate that the spin semiconductors provide a unique class of materials to exhibit exceptionally good spin thermoelectric (TE) properties, characterized by unprecedented giant S_s and Z_sT values, mainly because the spin Seebeck coefficient is found to increase linearly with the increasing spin gap.

Besides this key *spin-dependent* property of large spin gap we discover here, there are other known *spin-independent* properties favored by conventional high-ZT materials which can also be beneficial for spin caloritronics materials. First, a large band gap usually guarantees high specific heat of carriers, which is part of the reason why the best TE materials are mostly semiconducting [11]. Second, a narrow band around the Fermi energy leads to rapid variation of transmission function in the energy window of interest and hence good TE performance, as shown in quantum dots [12,13]. For these reasons, GNRs with antidots [9] have been recently shown to exhibit large S_s and Z_sT if they were assumed to be ferromagnetic instead of their paramagnetic ground state [14]. (We note that spin figure of merit in a nonmagnetic material is zero because of spin degeneracy. So, ferromagnetism is a mandatory condition for spin caloritronics effect, but it is not a tunable property for increasing spin figure of merit.) Surprisingly, however, we found that the maximum room-temperature S_s and Z_sT of ST GNRs are 5 and 50 times larger than those of GNRs with antidots [15], respectively. This is because besides the common spin-independent features of large band gap and narrow bandwidth, the ST GNRs with a ferromagnetic ground state have a special spin-dependent property of large spin gap not possessed by the GNRs with antidots which are usually ferromagnetic metals without spin gap.

Specifically, our first-principles and tight-binding (TB) calculations show that the S_s of ST GNRs is generally of the order of mV/K and Z_sT can be as high as over 100. For example, a ST GNR with a size of (4,4) [see size definition in Fig. 1(a)] can exhibit room-temperature S_s and Z_sT as high as 3.4 mV/K and 119, respectively. The key to achieving such giant spin caloritronic effect is the special property possessed by the spin semiconductors, a finite spin gap, with S_s increasing linearly with the increasing spin gap. Also, S_s is nearly a constant when chemical potential is located inside the spin gap, indicating the robustness of high S_s against charge doping that shifts the Fermi energy, which can be a useful feature in real applications. S_s and G_s are decoupled when the chemical potential is inside the spin gap, so it is highly possible for them to be tuned separately; energy states of different spins of ST GNRs near the Fermi energy can be separated in energy and spatially, which is advantageous for spin manipulation and detection. Additional benefit comes from the fact that thermal conduction in ST GNRs is naturally reduced by edge roughness and narrow ribbon width [16,17], which restrict phonon conduction.

Our calculations for electronic structures are performed within density-functional theory in the

*dwh@phys.tsinghua.edu.cn
†fliu@eng.utah.edu

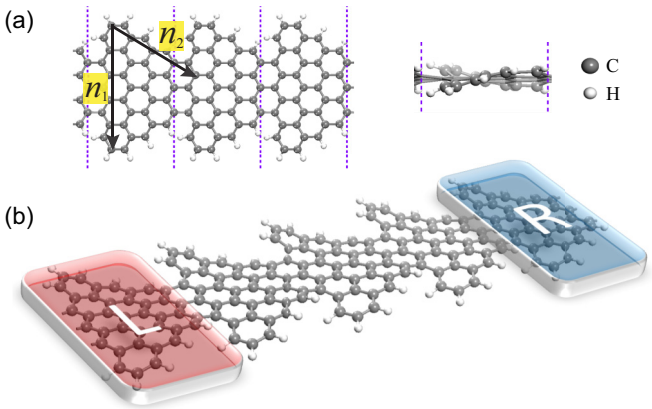

FIG. 1. (Color online) (a) A top (left) and side view (right) of a (n_1,n_2) ST GNR, where $n_1 = 5$ and $n_2 = 4$ denote the size of the ST GNR. Carbon and hydrogen atoms are in gray (large) and white (small), respectively. Violet dashed lines indicate the division of unit cells. (b) A ST GNR is divided into left (L), right (R) thermal contacts, and the center region for calculation of thermal transport.

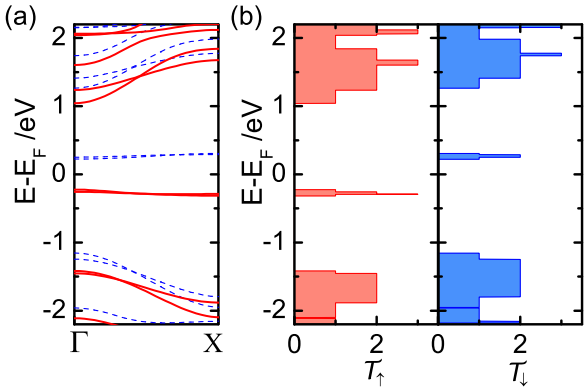

FIG. 2. (Color online) (a) Spin-polarized band structure of ferromagnetic (5,4) ST GNR. Spin-up and -down bands are denoted by red solid and blue dashed lines, respectively. The Fermi energy is set to the middle of the spin gap. (b) Transmission of spin-up (left panel) and -down (right panel) electrons.

Perdew-Burke-Ernzerhof generalized gradient approximation, as implemented in the Vienna *ab initio* simulation package [18]. All structures are built with vacuum space larger than 10 Å and are fully relaxed until forces on atoms are less than 0.01 eV/Å using total energy minimization. Plane-wave cutoff of 600 eV and a Monkhorst-Pack k-point mesh of $11 \times 1 \times 1$ are used for geometry optimization and electronic structure calculations. Transmission function of individual spin channels $\mathcal{T}_\sigma(\varepsilon)$ are obtained by counting bands [19].

For thermal transport calculations, a supercell system is divided into three regions: left and right contacts, and central region, as shown in Fig. 1(b). After obtaining the force constants of the two-probe system using a second-generation reactive empirical bond order potential [20] within the general utility lattice program [21], the phonon nonequilibrium Green's function method is applied to get phonon transmission $\Xi(\omega)$, where ω is the phonon frequency. Afterwards, we use Landauer-Büttiker formalism to get quasiballistic thermal conductance [16,22]:

$$\kappa_{ph} = \frac{k_B^2 T}{h} \int_0^\infty dx \frac{x^2 e^x}{(e^x - 1)^2} \Xi\left(\frac{k_B T}{\hbar} x\right), \tag{1}$$

where k_B is Boltzmann constant, h is Planck constant, $\hbar = h/2\pi$, and T is absolute temperature. In light of the long spin-relaxation length in graphene ($\sim$2 μm), spin relaxation in ideal ST GNRs can be ignored [9,23]. Then, with electronic transmission and thermal conductance at hand, we can calculate spin TE properties (i.e., S_s, G_s, and Z_sT) by virtue of the following quantities [24]:

$$G_\sigma = e^2 L_{0\sigma}, \tag{2}$$

$$S_\sigma = -\frac{1}{eT} \frac{L_{1\sigma}}{L_{0\sigma}}, \tag{3}$$

$$\kappa_{e,\sigma} = \frac{1}{T}\left(L_{2\sigma} - \frac{L_{1\sigma}^2}{L_{0\sigma}}\right), \tag{4}$$

with e being the elementary charge, f the Fermi-Dirac distribution, $\sigma = \uparrow, \downarrow$, and

$$L_{n\sigma} \equiv \frac{1}{h} \int d\varepsilon (\varepsilon - \mu)^n (-f'_\varepsilon)|_{\mu,T} \mathcal{T}_\sigma(\varepsilon). \tag{5}$$

The reference electrochemical potential μ and temperature T are set as $\mu = \frac{1}{4}(\mu_{L\uparrow} + \mu_{L\downarrow} + \mu_{R\uparrow} + \mu_{R\downarrow})$ and $T = \frac{1}{2}(T_L + T_R)$.

First, we investigate the spin TE properties of a (5,4) ST GNR with hydrogen-saturated edges. Figure 1(a) shows its optimized structure. This buckling configuration is energetically more stable than the previously studied planar structure [10] by 1.065 eV per unit cell, because the buckling reduces the steric repulsion between two neighboring H atoms at the inner corner of the ST edges. The optimized lattice constant is $a_0 = 8.587$ Å, which is slightly shorter than that of the planar structure. The ST edge is purposely designed to have an angle of 120° between any two zigzag edge orientations, so that its ground state is ferromagnetic [14], which has a lower energy than the paramagnetic and antiferromagnetic states by 232 meV and 145 meV per unit cell, respectively.

ST GNRs have some common useful features in their distinctive electronic band structures, as illustrated in Fig. 2(a). There are four localized energy bands around the Fermi level: two occupied spin-up valence bands and two empty spin-down conduction bands, giving rise to a net magnetic moment of $2\mu_B$ per unit cell. Similar to zigzag GNRs, these localized bands are edge states [10,25]. Specific for spin-semiconducting ST GNRs, the spin-up and -down edge states are separated by a spin gap, which is 0.447 eV in a (5,4) ST GNR.

With the calculated band structure, spin-polarized transmission function can be obtained using a band-counting method [19], as plotted in Fig. 2(b). Localized bands lead to narrow peaks in transmission, which is bad for electronic conductance, but good for obtaining large Seebeck coefficients [26,27]. Away from the band gap, bands are dispersive and more extended in real space. Since spin relaxation is absent, electrons see only one set of bands with the same spin. In this case, individual band gaps for a (5,4) ST GNR are $E_{g\uparrow} = 1.266$ eV and $E_{g\downarrow} = 1.378$ eV, respectively. Therefore, spin

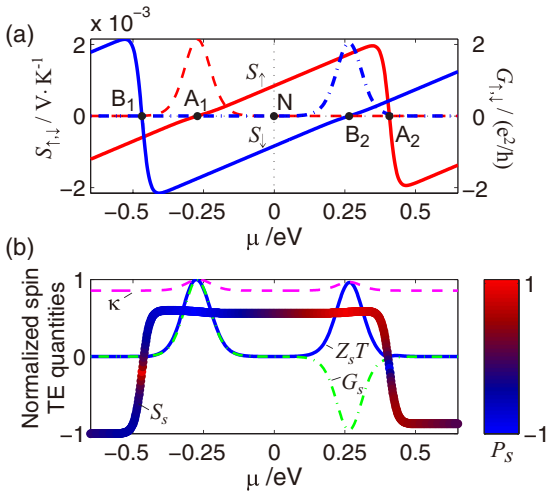

FIG. 3. (Color online) Room-temperature spin TE properties of a (5,4) ST GNR. (a) Spin-up (red solid line) and -down (blue solid line) Seebeck coefficients. Spin-up (red dashed line) and -down (blue dashed-dotted line) conductances are also shown. (b) Normalized spin caloritronic properties as a function of chemical potential, with the zero potential set to the middle of the spin gap. The normalization factors are $Z_sT = 95.6$, $S_s = 2.98$ mV/K, and $G_s = 8.30 \times 10^{-5}$ Siemens, respectively, and $\kappa = 0.794$ nW/K. Colors of Seebeck coefficients in (b) change according to Seebeck polarization, $P_S = (|S_\uparrow| - |S_\downarrow|)/(|S_\uparrow| + |S_\downarrow|)$.

independency in this system results in an about threefold increase in band gaps for individual spin channels.

The existence of spin gap indicates different specific heat of spin carriers, leading to different transmission for different spin channels. It can be readily shown that the spin Seebeck coefficient S_s scales linearly with the spin gap [28]. Therefore, the ST GNRs with a spin gap plus band localization are expected to have excellent spin TE properties. In Fig. 3(a), we plot room-temperature S_σ. In the given energy range, both $S_\uparrow$ and $S_\downarrow$ have a maximum absolute value of around 2 mV/K. Notice that this value is even bigger than those of Bi_2Te_3 (bulk [29]: 70.5 μV/K for n type, 227 μV/K for p type; thin film [30]: 247 μV/K), which is one of the best TE materials, by one order of magnitude. We note that $S_\uparrow = 0$ at $\mu = -0.272$ and 0.408 eV, which are denoted as A_1 and A_2 points in Fig. 3(a). At these points, thermal gradient induces only a spin-down current and Z_sT is as high as 95.6 at the A_1 point [see Fig. 3(b)], which can be attributed to the flatness of S_s and little variation of thermal conduction (hence the coincidence of outlines of Z_sT and G_s) and the fact that $S_\uparrow$ has zero values at the symmetry center of conductance due to the odd-symmetric integration kernel in Eq. (3). Therefore, a 100% polarized spin current can be generated at $\mu = -0.272$ eV (A_1 point) using thermal gradient, with a process of $Z_sT = 95.6$. On the left-/right-hand side of A_1, $S_\uparrow$ is negative/positive due to n-/p-type-like transport [31,32]. $S_\uparrow$ gradually becomes negative on the right side far from the spin-up transmission peak. This can be attributed to the contribution of bulk conduction bands. Around the spin-up edge bands, $S_\uparrow$ varies linearly, where the maximum absolute value is approximately proportional to the spin-up band gap [31].

$S_\downarrow$ has a similar but antisymmetric trend with that of $S_\uparrow$. Correspondingly, $S_\downarrow$ reaches zero at -0.468 and 0.265 eV, denoted as B_1 and B_2 points in Fig. 3(a), respectively. High Z_sT can also be realized at B_2, where only accumulation of spin-up electrons will be induced by a thermal gradient. It is interesting to point out that $S_\uparrow = -S_\downarrow$ at the N point [$\mu \approx -0.002$ eV; see Fig. 3(a)], where the induced charge voltage is zero but spin voltage $V_s = S_s\Delta T \neq 0$ in an open circuit. Under this situation, a thermal gradient induces only a pure spin accumulation without charge accumulation. It is worth noting that the N point is the so-called neutral point, where contributions from holes and electrons cancel with each other; it is supposed to be at $\mu = 0$ when the transmission functions are exactly symmetric [11,33].

Further as shown in Fig. 3(b), S_s is rather flat inside the spin gap and across the localized bands. This can be inferred from Fig. 3(a), where $S_\uparrow$ and $S_\downarrow$ have an almost constant difference due to the inversely symmetric Seebeck coefficients between two spin channels and their linear dependence on chemical potential in between two transmission peaks. The flatness of S_s implies a decoupling of S_s and G_s, which can be useful for improving spin TE performance because overall Z_sT can be enhanced by increasing S_s or G_s independently. Such decoupling is difficult for charge TE effect, because Seebeck coefficient S and electric conductance G generally have opposite trends against the carrier density [11]. Besides its flatness, S_s is positive around and between the two transmission peaks. This indicates that the sign of S_s has nothing to do with carrier types, noticeably different from S_σ. Also, it is shown that S_s has more contribution from spin-down electrons when $\mu < 0$ and vice versa. Experimentally, S_s is only -3.8 μV/K for Permalloy and -1.8 μV/K for cobalt [4,34]. The maximum absolute value of S_s of a (5,4) ST GNR is about 3.0 mV/K, while the inside-band-gap value is 1.68 mV/K; both are two to three orders of magnitude larger than that of Permalloy.

As shown in Fig. 3(b) thermal conductance changes little as the chemical potential varies, and is mostly contributed by phonons (over 80%). And it is worth noting that without electron-phonon interaction, lattice thermal conductance is independent of μ and electronic thermal conductance is almost zero off conductance peaks.

Giant S_s and Z_sT are expected in most ST GNRs with the common features of spin gap and narrow bands. To confirm this, we now turn to calculations using the TB Hubbard model [10,35], so that ST GNRs of different sizes can be systematically studied. The Hamiltonian can be written as

$$H = t \sum_{\langle i,j\rangle,\sigma} c^\dagger_{i\sigma}\, c_{j\sigma} + U \sum_{i,\sigma} (\langle n_{i\bar{\sigma}}\rangle - 1/2)\, n_{i\sigma}, \qquad (6)$$

where $c^\dagger_{i\sigma}$ ($c_{i\sigma}$) creates (annihilates) a spin-σ electron at site i, $n_{i\sigma} = c^\dagger_{i\sigma} c_{i\sigma}$ ($\langle n_{i\sigma}\rangle$) counts the number (average number) of spin-σ electrons at site i, t is the hopping energy between two nearest-neighbor carbon atoms, and U is the on-site Coulomb repulsion. $\langle n_{i\sigma}\rangle$ is obtained self-consistently from

$$\langle n_{i\sigma}\rangle = \int_{-\infty}^{E_F} g_{i\sigma}(E)\, dE, \qquad (7)$$

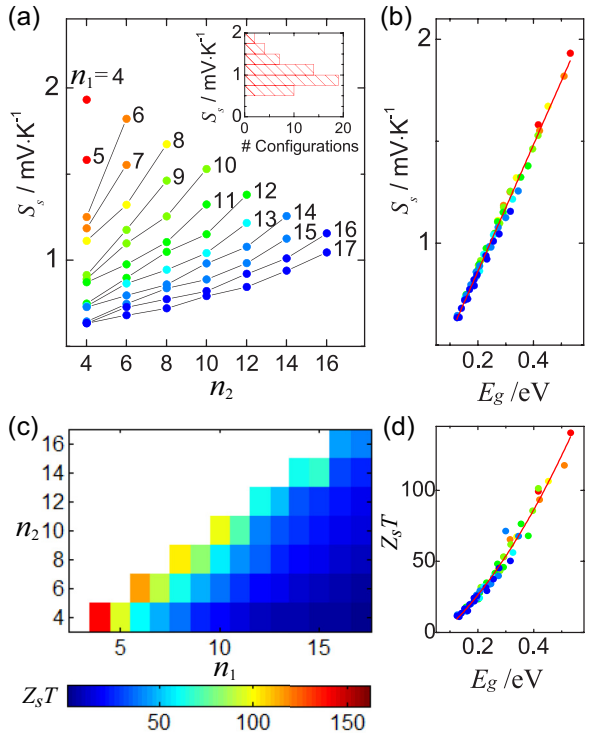

FIG. 4. (Color online) Room-temperature S_s and Z_sT of (n_1,n_2) ST GNRs, as calculated from the TB model. (a) $S_s(\mu = 0)$ of (n_1,n_2) ST GNR as a function of n_2 with $4 \leqslant n_1 \leqslant 17$. Data with the same n_1 are line connected for clarity. Inset: Statistical distribution of S_s. (b) Room-temperature S_s (solid circles) plotted as a function of E_g. The red solid line is a linear fit to the data. (c) Maximum Z_sT of (n_1,n_2) ST GNRs with $4 \leqslant n_1 \leqslant 17$ and $n_2 = 4,6,\ldots,16$. (d) Maximum Z_sT (circles) are plotted as a function of E_g. The red solid line is a quadratic fit to the data. Also note that for ST GNRs as shown in Fig. 1, we have $n_1 \geqslant n_2$ and n_2 to be even.

where $g_{i\sigma}$ is the local density of states. It is found that first-principles band structure of a buckling (5,4) ST GNR can be very well reproduced using $U = 3$ eV and $t = -2.6$ eV. Note that the U value here is different from Ref. [13] because of a buckled structure having less dispersive bands around the Fermi energy.

Results calculated from the TB model are presented in Fig. 4. Figure 4(a) shows that $S_s(\mu = 0)$ increases with n_2 monotonically for a given n_1, and decreases with n_1 for a given n_2. Among the total 56 configurations studied, 27 of them have an S_s value larger than 1 mV/K and all of them larger than 0.5 mV/K. The (4,4) ST GNR is found to have the largest in-gap S_s of 1.9 mV/K. Away from the band gap, S_s can be enhanced further [see Fig. 3(b)], and the maximum S_s is about 3.4 mV/K, which is further confirmed by *ab initio* calculations. However, S_s far away from the transmission peaks of localized bands corresponds to low Z_sT, while S_s near the peaks, almost equal to $S_s(\mu = 0)$, corresponds to high Z_sT. The TB model calculations clearly confirm the linear dependence of S_s on spin gap E_g, as illustrated in Fig. 4(b), which is also consistent with the linear variation of S_σ inside E_g as shown in Fig. 3(a).

ST GNRs with close n_1 and n_2, which have a bigger sawtooth and narrower connection region, are found to have larger Z_sT, as shown in Fig. 4(c). In particular, the best value of Z_sT is found in the (4,4) ST GNR, which is also confirmed to be 119 by *ab initio* calculations. When increasing n_1 without changing n_2, Z_sT decreases rapidly, which can be attributed to the monotonic decrease of band gaps and near-linear increase of thermal conductance due to the increase of the narrowest part of the ribbon width [17]. In contrast, increasing n_2 without changing n_1, the structure becomes more sawtoothlike, and its Z_sT increases fast. The lowest Z_sT in Fig. 4(c) comes from (17,4) ST GNR, which is still as high as 4.5. Interestingly, Z_sT has roughly a quadratic dependence on spin gap, as shown in Fig. 4(d), which is again consistent with the linear dependence of S_s on E_g.

In summary, we demonstrate that spin semiconductors can be excellent spin TE materials. In particular, giant spin caloritronic effects are expected in spin-semiconducting nanostructures due to additional benefits of narrow bandwidth and reduced thermal conductance. The largest S_s (~3.4 mV/K) and Z_sT (~119) values are found in the model systems of ST GNRs. It is further shown that S_s increases linearly with the spin gap. Also, S_s, being decoupled from G_s, is almost independent of chemical potential within the spin gap, so that the giant spin caloritronic effects are robust against doping in a device setting. Our studies show promise for thermal generation of 100% spin-polarized currents at room temperature with high efficiency, paving the way towards real applications for spin caloritronics.

We thank Zhengfei Wang, Fawei Zheng, Bing Huang, and Huaqing Huang for helpful discussions. X.C., W.D., and B.G. gratefully acknowledge financial support from MST-China (Grants No. 2011CB921901 and No. 2011CB606405) and the NSF-China (Grant No. 11334006). X.C. is thankful to FRQNT for a PBEEE fellowship. F.L. acknowledges support by U.S. DOE-BES (Grant No. DE-FG02-04ER46148).

[1] S. Wolf, D. Awschalom, R. Buhrman, J. Daughton, S. Von Molnar, M. Roukes, A. Y. Chtchelkanova, and D. Treger, Science **294**, 1488 (2001).
[2] J. Maassen, W. Ji, and H. Guo, Nano Lett. **11**, 151 (2011).
[3] K. Uchida, S. Takahashi, K. Harii, J. Ieda, W. Koshibae, K. Ando, S. Maekawa, and E. Saitoh, Nature (London) **455**, 778 (2008).
[4] A. Slachter, F. Bakker, J. Adam, and B. van Wees, Nat. Phys. **6**, 879 (2010).
[5] J. Le Breton, S. Sharma, H. Saito, S. Yuasa, and R. Jansen, Nature (London) **475**, 82 (2011).
[6] G. E. W. Bauer, E. Saitoh, and B. J. van Wees, Nat. Mater. **11**, 391 (2012).
[7] Y. Dubi and M. Di Ventra, Phys. Rev. B **79**, 081302 (2009).
[8] J. Zheng, F. Chi, and Y. Guo, J. Phys.: Condens. Matter **24**, 265301 (2012).
[9] M. Wierzbicki, R. Swirkowicz, and J. Barnaś, Phys. Rev. B **88**, 235434 (2013).

[10] Z. F. Wang, S. Jin, and F. Liu, Phys. Rev. Lett. **111**, 096803 (2013).
[11] G. J. Snyder and E. S. Toberer, Nat. Mater. **7**, 105 (2008).
[12] P. Murphy, S. Mukerjee, and J. Moore, Phys. Rev. B **78**, 161406 (2008).
[13] J. P. Heremans, V. Jovovic, E. S. Toberer, A. Saramat, K. Kurosaki, A. Charoenphakdee, S. Yamanaka, and G. J. Snyder, Science **321**, 554 (2008).
[14] D. Yu, E. M. Lupton, H. Gao, C. Zhang, and F. Liu, Nano Res. **1**, 497 (2008).
[15] We note that there is a factor of 1/2 difference in the definition of S_s between our work and Ref. [9], and the difference has been taken into account for comparison.
[16] Y. Xu, X. Chen, J.-S. Wang, B.-L. Gu, and W. Duan, Phys. Rev. B **81**, 195425 (2010).
[17] X. Chen, Y. Xu, X. Zou, B.-L. Gu, and W. Duan, Phys. Rev. B **87**, 155438 (2013).
[18] J. P. Perdew, K. Burke, and M. Ernzerhof, Phys. Rev. Lett. **77**, 3865 (1996).
[19] C. Jeong, R. Kim, M. Luisier, S. Datta, and M. Lundstrom, J. Appl. Phys. **107**, 023707 (2010).
[20] D. W. Brenner, O. A. Shenderova, J. A. Harrison, S. J. Stuart, B. Ni, and S. B. Sinnott, J. Phys.: Condens. Matter **14**, 783 (2002).
[21] J. Gale, J. Chem. Soc., Faraday Trans. **93**, 629 (1997).
[22] Y. Xu, Z. Li, and W. Duan, Small **10**, 2182 (2014).
[23] T. Maassen, J. J. van den Berg, N. Ijbema, F. Fromm, T. Seyller, R. Yakimova, and B. J. van Wees, Nano Lett. **12**, 1498 (2012).
[24] X. Chen, D. Liu, W. Duan, and H. Guo, Phys. Rev. B **87**, 085427 (2013).
[25] K. Nakada, M. Fujita, G. Dresselhaus, and M. S. Dresselhaus, Phys. Rev. B **54**, 17954 (1996).
[26] M. Paulsson and S. Datta, Phys. Rev. B **67**, 241403 (2003).
[27] P. Reddy, S.-Y. Jang, R. A. Segalman, and A. Majumdar, Science **315**, 1568 (2007).
[28] See Supplemental Material at http://link.aps.org/supplemental/10.1103/PhysRevB.90.121403 for the E_g dependence of S_s.
[29] *CRC Handbook of Thermoelectrics*, edited by D. M. Rowe (CRC Press, Boca Raton, FL, 1995).
[30] V. Goyal, D. Teweldebrhan, and A. A. Balandin, Appl. Phys. Lett. **97**, 133117 (2010).
[31] Y. Ouyang and J. Guo, Appl. Phys. Lett. **94**, 263107 (2009).
[32] S. Datta, *Quantum Transport: Atom to Transistor* (Cambridge University Press, Cambridge, UK, 2005).
[33] T. Rejec, R. Žitko, J. Mravlje, and A. Ramšak, Phys. Rev. B **85**, 085117 (2012).
[34] F. K. Dejene, J. Flipse, and B. J. van Wees, Phys. Rev. B **86**, 024436 (2012).
[35] J. Guo, D. Gunlycke, and C. T. White, Appl. Phys. Lett. **92**, 163109 (2008).